BIOCHEMISTRY
including biophysical chemistry & molecular biology

Article

pubs.acs.org/biochemistry

Molecular Dynamics Investigation of the Substrate Binding Mechanism in Carboxylesterase

Qi Chen,[†] Zheng-Jiao Luan,[†] Xiaolin Cheng,*[,‡,§] and Jian-He Xu*[,†,∥]

[†]State Key Laboratory of Bioreactor Engineering, East China University of Science, Technology, Shanghai 200237, China

[‡]UT/ORNL Center for Molecular Biophysics, Oak Ridge National Laboratory, Oak Ridge, Tennessee 37831, United States

[§]Department of Biochemistry and Cellular and Molecular Biology, University of Tennessee, Knoxville, Tennessee 37996, United States

[∥]Shanghai Collaborative Innovation Center for Biomanufacturing, East China University of Science and Technology, Shanghai 200237, China

Supporting Information

ABSTRACT: A recombinant carboxylesterase, cloned from *Pseudomonas putida* and designated as rPPE, is capable of catalyzing the bioresolution of racemic 2-acetoxy-2-(2′-chlorophenyl)acetate (*rac*-AcO-CPA) with excellent (*S*)-enantioselectivity. Semirational design of the enzyme showed that the W187H variant could increase the activity by ∼100-fold compared to the wild type (WT) enzyme. In this study, we performed all-atom molecular dynamics (MD) simulations of both apo-rPPE and rPPE in complex with (*S*)-AcO-CPA to gain insights into the origin of the increased catalysis in the W187H mutant. Our results show differential binding of (*S*)-AcO-CPA in the WT and W187H enzymes, especially the interactions of the substrate with the two active site residues Ser159 and His286. The replacement of Trp187 by His leads to considerable structural rearrangement in the active site of W187H. Unlike in the WT rPPE, the cap domain in the W187 mutant shows an open conformation in the simulations of both apo and substrate-bound enzymes. This open conformation exposes the catalytic triad to the solvent through a water accessible channel, which may facilitate the entry of the substrate and/or the exit of the product. Binding free energy calculations confirmed that the substrate binds more strongly in W187H than in WT. On the basis of these computational results, we further predicted that the mutations W187Y and D287G might also be able to increase the substrate binding and thus improve the enzyme's catalytic efficiency. Experimental binding and kinetic assays on W187Y and D287G show improved catalytic efficiency over WT, but not W187H. Contrary to our prediction, W187Y shows slightly decreased substrate binding coupled with a 100-fold increase in turnover rate, while in D287G the substrate binding is 8 times stronger but with a slightly reduced turnover rate. Our work provides important molecular-level insights into the binding of the (*S*)-AcO-CPA substrate to carboxylesterase rPPEs, which will help guide future development of more efficient rPPE variants.

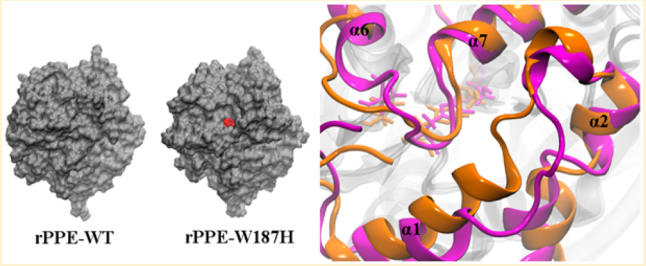

Carboxylesterases (EC 3.1.1.1) are members of the α/β hydrolase family which have been found widely distributed in animals, plants, and microorganisms.[1] They can hydrolyze numerous structurally diverse compounds that contain a specific functional group, such as amide, thioester, carboxylic acid ester, and so on. Because of their broad substrate spectrum, carboxylesterases are widely used as biocatalysts for the synthesis of important materials in pharmaceutical and chemical industries.[2]

The research on catalytic mechanism and enzyme improvement has advanced significantly by the exploitation of structure-based and rational design methods.[3−7] Important mutations that affect the enzymatic activity can be identified through structural analysis as the "hot spots". Site-directed mutagenesis and saturated mutation experiments can then be performed to search for enzymes with improved catalytic efficiency and/or suitability for industrial applications.

In our previous work, a recombinant carboxylesterase, cloned from *Pseudomonas putida* and designated as rPPE, is found to be capable of catalyzing the bioresolution of racemic 2-acetoxy-2-(2′-chlorophenyl)acetate (*rac*-AcO-CPA) with excellent (*S*)-enantioselectivity,[8] as shown in Figure S1, Supporting Information. (*S*)-AcO-CPA is a crucial chiral intermediate for the synthesis of a widely prescribed drug named Clopidogrel (Plavix) for antiplatelet therapy.[9] The wild type rPPE has a very low activity on *rac*-AcO-CPA, but our previous experimental studies showed that the W187H mutant increases the enzymatic activity by ∼100-fold compared to the wild type, which significantly improves the potential of industrial application of this recombinant enzyme.[10]

Received: December 27, 2014
Revised: February 18, 2015
Published: February 25, 2015

DOI: 10.1021/bi5015612
Biochemistry 2015, 54, 1841−1848

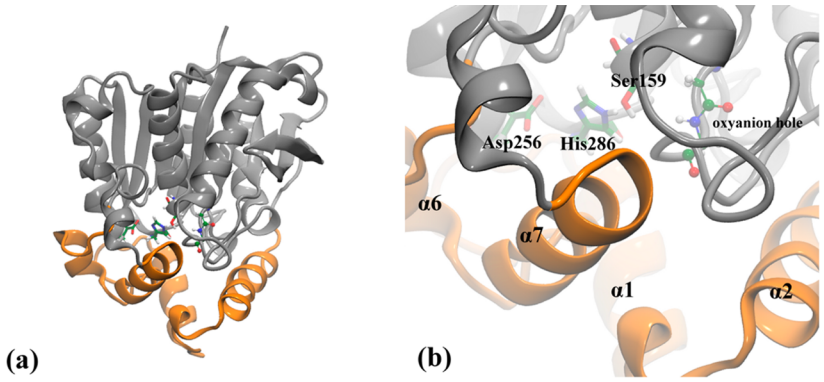

Figure 1. Crystal structure (a) and active site (b) of apo-form rPPE. α Helices, β strands, and loops are represented by helical ribbons, arrows and ropes, respectively. The catalytic triad is represented by sticks and labeled. The overall α/β hydrolase fold is shown in gray and the cap domain is shown in orange.

The crystal structures of the apo rPPE, the W187H mutant and the W187H mutant complexed with the substrate (*S*)-AcO-CPA have been determined recently.[11] The overall structure of rPPE (Figure 1) shows an α/β hydrolase fold together with a cap domain, similar to other enzymes in the hormone sensitive lipase (HSL) family.[12] The cap domain is formed by the clustering of two *N*-terminal α-helices (α1 and α2) and two other α-helices (α6 and α7). The conserved catalytic triad consists of Ser159, Asp256, and His286. Compared to the crystal structure of WT rPPE, the side chain of His187 in W187H has shifted by about 2.3 Å, which may provide an explanation for the improved catalytic efficiency in the W187H mutant. However, the molecular details on how this W187H mutation may affect the enzyme activity remains elusive only by inspecting these static structures.

Several catalytic mechanisms of different carboxylesterases have been proposed. Ross's group proposed a "side door" mechanism in mammalian carboxylesterases (CEs) that may govern the entry of the substrate and the exit of the product.[13] From the analysis of the crystal structure of a *Bacillus subtilis* CE (pnb-CE), the "side-door" residues were found to be important for the metabolism of a water-soluble anticancer prodrug CPT-11 (7-ethyl-10-[4-(1-piperidino)-1-piperidino]-carbonyloxycamptothecin).[14] All-atom MD simulation of pnb-CE by Wadkins et al. has shown that the dynamic motions of coil_5 (residues 61−82) and coil_21 (residues 408−422) located on the surface of pnbCE are critical to the substrate binding.[15]

Here, we performed all-atom MD simulations of the wild type and mutant rPPE enzymes, both apo and in complex with (*S*)-AcO-CPA, to investigate the binding mechanisms of the substrate in different enzymes. Our studies provide insights into why the catalytic activity of the W187H mutant has increased from the perspective of the substrate binding. Based on these insights along with additional Molecular Mechanics−Poisson−Boltzmann (Generalized Born)/Surface Area (MM-PB(GB)/SA) binding energy results, we predicted that the W187Y and D287G mutants might have increased catalytic efficiency given their potentially improved substrate binding than the WT and W187H enzymes. Finally, experimental site-directed mutagenesis and biochemical assays were employed to verify the importance of the "hot spots" for the substrate binding predicted by our MD simulations.

MATERIALS AND METHODS

Molecular Dynamics Simulation. The X-ray crystal structures of the wild type rPPE (APO-WT, PDB: 4OB8), the W187H mutant (APO-W187H, PDB: 4OB7), and the W187H mutant complexed with the substrate (*S*)-AcO-CPA (rPPE-W187H, PDB: 4OB6) have been resolved recently.[11] Auto Dock Vina was used to obtain a starting structure of the wild type rPPE in complex with the substrate (rPPE-WT), where the APO-WT structure was used for the ligand docking.[16] To ensure convergence of the simulations, we also built another starting structure of the substrate-bound wild type complex named as rPPE-WT-parallel, which was generated by mutating H187 back to W187 in the rPPE-W187H structure (PDB: 4OB6). All these five structures were then used as the initial models for the all-atom MD simulations.

LEaP module in Amber11 was used to add missing atoms and hydrogen atoms.[17] Each system was solvated in a TIP3P water box and extended by a thickness of 15 Å on each side of the protein.[18] The final five systems each contain 317 residues and ∼50 000 atoms. The Amber FF99SB force field was used for the protein.[19] The force field parameters of the substrate (*S*)-AcO−CPA were generated via the Antechamber package and the partial charges were calculated with the RESP method.[20,21] The ligand force field parameters are listed in Table S1, Supporting Information.

All the simulations were performed using NAMD v2.9.[22] Each system was minimized following four steps: step 1, fix all nonwater atoms, minimize water only; step 2, minimize water and all hydrogen atoms in protein; step 3, fix protein backbone atoms and minimize everything else; and step 4, minimize all the atoms in the system. Each step consists of 5000 minimization steps. After minimization, each of the simulation systems was heated gradually from 0 K to 300 K in the NVT ensemble by Langevin dynamics followed by 2 ns of equilibration and 50 ns of NPT production simulations. The van der Waals (vdW) interactions were treated with a smooth cutoff of 10.5−12.0 Å using a switching function. The particle-mesh Ewald (PME) method was employed to compute the long-range electrostatic interactions with a 1.0 Å grid spacing.[23] The integration step is 2 fs, and the coordinates were saved every 2 ps.

Trajectory analyses, including the root-mean-square deviation (RMSD), root-mean-square fluctuation (RMSF), structural clustering and principal component analysis (PCA), were performed using the Gromacs 4.5.5 program.[24] The R package

DOI: 10.1021/bi5015612
Biochemistry 2015, 54, 1841−1848

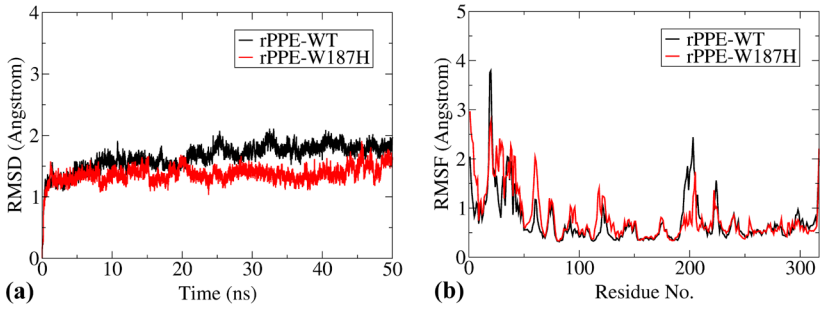

Figure 2. RMSD (a) and RMSF (b) results of WT (black) and W187H (red) rPPEs in complex with the substrate (*S*)-AcO−CPA.

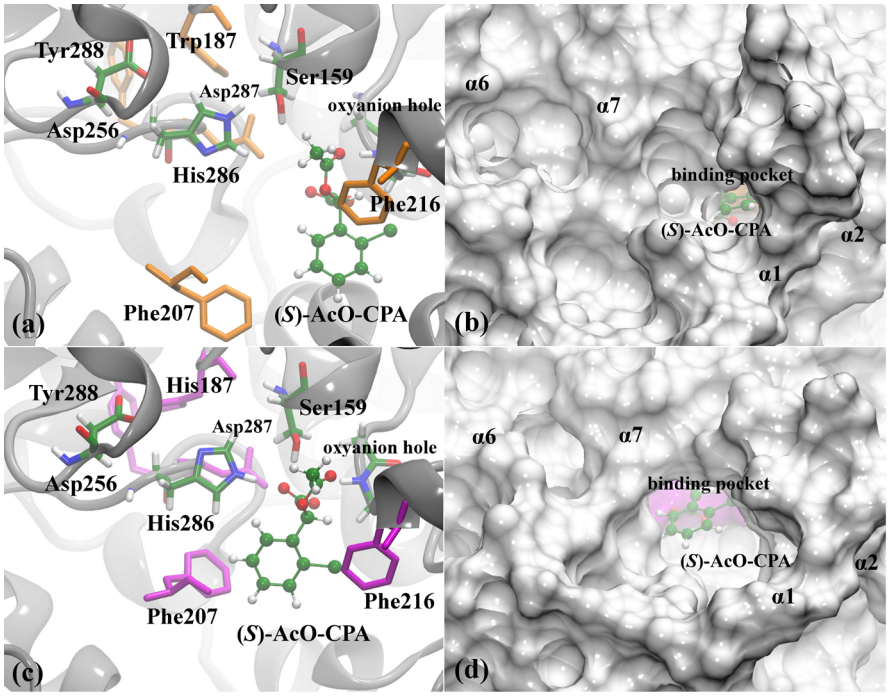

Figure 3. Binding modes of the substrate in the WT (a) and W187H mutant (c) rPPEs; binding pocket in the WT (b) and W187H mutant (d) rPPEs. The catalytic triad and the substrate (*S*)-AcO-CPA are shown in green, and other relevant residues are shown in orange (WT) and purple (W187H), respectively.

Bio3D utilities were employed for correlation matrix calculation and analysis.[25] Visualization and figures of protein structures were generated with VMD.[26]

MM-PB(GB)/SA methods from Amber were used to quantify the binding free energy for the substrate in both WT and W187H enzymes.[27−29] The calculation principle of MM-PB(GB)/SA can be described as follows.

$$\Delta G_{bind} = G_{complex} - G_{receptor} - G_{ligand} \quad (1)$$

$$G = E_{MM} + G_{PB} + G_{nonpolar} - TS \quad (2)$$

$$E_{MM} = E_{bond} + E_{angle} + E_{torsion} + E_{improper} + E_{vdW} + E_{elec} \quad (3)$$

From eq 1, the total binding free energy change for a protein−ligand system (ΔG_{bind}) is defined as the difference between the free energies of the complex ($G_{complex}$), the receptor ($G_{receptor}$), and the ligand (G_{ligand}). Each free energy term is calculated as the sum of the internal energy (E_{MM}) in the gas phase, the solvation free energy comprised of an electrostatic term (G_{PB} or G_{GB}) and a nonpolar component ($G_{nonpolar}$), and the entropy (TS). As shown in eq 3, E_{MM} consists of energies from bonded interactions (E_{bond}, E_{angle}, $E_{torsion}$, $E_{improper}$) and nonbonded interactions (the van der Waals E_{vdW}, the electrostatic E_{elec}). The nonpolar component of the solvation free energy $G_{nonpolar}$ was estimated by the molecular solvent accessible surface area (SASA).

Site-Directed Mutagenesis. Site-directed mutations were constructed by Quick Change Site-Directed Mutagenesis kit, and the plasmid pET21a(+) containing the gene of rPPE was used as the template. Primers used for the mutations are listed in Table S3, Supporting Information. The PCR products were then transformed into *Escherichia coli* BL21 (DE3) for esterase expression. Cultivation of the recombinant *E. coli* cells expressing rPPE or its mutants and enzyme purification using Ni^{2+} affinity chromatography were performed as described previously.[8]

The enzymatic activity toward acetoxy acid (with K^+ as the counterion) was analyzed using HPLC. One unit of enzyme activity was defined as the amount of enzyme required for releasing 1.0 μmol of hydroxy acid per minute under the assay conditions. The reaction was performed in potassium phosphate buffer (pH 6.5, 50 mM) at 30 °C. The kinetic parameters of the purified variants (W187Y and D287G) on

DOI: 10.1021/bi5015612
Biochemistry 2015, 54, 1841−1848

the substrate were determined by measuring the activity under the varied substrate concentration (10−200 mM). The Michaelis−Menten constant (K_m) and the maximal reaction rate (V_{max}) of the enzyme were calculated from Lineweaver−Burk plots.

RESULTS

RMSD and RMSF Analysis. Figure 2a shows the RMSDs relative to their respective initial structures as a function of time in the simulations of the substrate bound rPPE-WT and rPPE-W187H. The RMSDs of the apo wild type and mutant enzymes are shown in Figure S2a. It is clear that all the four systems have reached equilibrium with a RMSD of about 2 Å after 20 ns. The RMSF results displayed in Figures 2b and S2b show significant fluctuations in the loop regions of the enzyme, such as residues 18−28 ("20-loop"), residues 55−60 ("50-loop") and residues 200−210 ("200-loop"). As the "200-loop" is located near the binding pocket (Figure 1), its structural fluctuation may directly affect the substrate binding and thus the catalytic activity of the enzyme, which will be discussed in more details below.

Binding Mode Analysis. According to the crystal structure of rPPE-W187H, the side chains of His187 and Asp287 undergo a significant positional shift, which expands the substrate-binding pocket.[11] However, this conformational change is not seen in the apo-W187H crystal structure. Nevertheless, we found that the structural movement of the His187 and Asp287 side chains can be maintained in the entire MD simulations of the W187H mutant. Notably, the binding mode of the substrate in W187H is significantly different from that in the wild type. As shown in Figure 3a, in the wild type enzyme, the indole group of Trp187 is hydrogen bonded with Asp287 as reported in the crystal structure.[11] However, no stable interactions could be noticed between the catalytic triad and the substrate during the rPPE-WT simulation. The oxygen atom of the carboxyl group in the substrate is coordinated with Gly87, and the aromatic ring of the substrate forms a $\pi-\pi$ stacking interaction with the benzene ring of Phe216. A similar binding mode (with ligand RMSD < 0.5 Å) can be found in the simulation of the rPPE-WT-parallel system as shown in Figure S3, which highlights the reproducibility of the MD simulations. Only the rPPE-WT simulation results are used for further analysis described below.

Figure 3c shows the binding mode of the substrate in the W187H mutant. The distinct binding modes observed in the wild type and W187H are accompanied by the rearrangement of the active site.[30] The imidazole moiety of His187 swings toward Asp256 and interacts with the side chains of Tyr288 and Asp256, leading to a structural rearrangement of the active site. A stable hydrogen bond is formed between the carboxyl group of the substrate and the imidazole ring of His286. The aromatic ring of the substrate is sandwiched between the two benzene rings of Phe207 and Phe216. Overall, the substrate appears to make more extensive interactions with the surrounding residues in W187H than in the WT. The catalytic triad of residues (Ser159-His286-Asp256) is highly conserved among carboxylesterases. According to the proposed catalytic mechanism, the OH group of Ser159 undergoes a nucleophilic attack on the carbonyl carbon atom of the substrate, generating a tetrahedral intermediate. A low-barrier hydrogen bond formed between Asp256 and His286 facilitates the nucleophilic attack.[31,32] The average distance between the OH group of Ser159 and the carbonyl carbon atom of the substrate during the entire simulation is 3.3 ± 0.3 Å in W187H compared to 3.9 ± 0.3 Å in wild type. Moreover, the nucleophilic attack angle "θ" defined in Figure S4 is 73° ± 9° in W187H and 63° ± 12° in wild type. The smaller distance and larger angle of the nucleophilic attack in the W187H mutant suggest that the W187H-substrate complex represents a more potential near-attack conformation (NAC) than the wild type enzyme complex. The NAC is thought to be a necessary state for the reactant to proceed to a transition state.[33] Therefore, in addition to a potentially stronger substrate binding, the observed conformational change of the catalytic triad in W187H may also increase the reaction rate. The substrate assumes a more "activated" conformation in the W187H mutant with the active site residues prearranged for the reaction.

Structural Dynamics of the Cap Domain. The cap domain, comprised of two *N*-terminal α-helices (α1 and α2) and two other α-helices (α6 and α7), functions as a gate to the active site of the enzyme as shown in Figure 1a. The cap domain has been shown to be very important for the substrate binding.[34,35] The cap domain assumes an "open" conformation in W187H as shown in Figure 4c. The open conformation

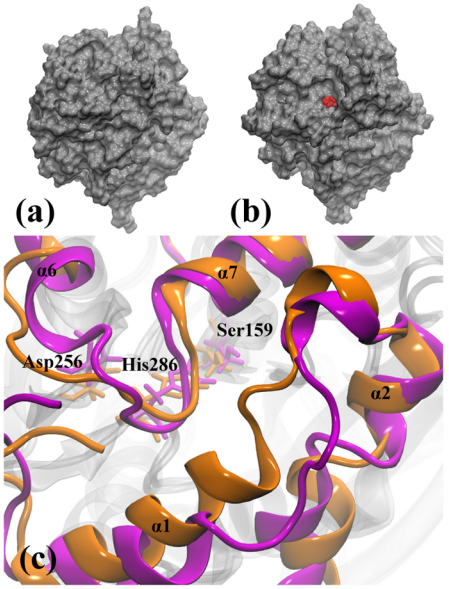

Figure 4. Surface view of the WT (a) and W187H (b) rPPEs. The distinct structures of the cap domain (c) in WT (orange) and W187H (purple) are superimposed.

exposes the catalytic triad to the solvent through a larger water accessible channel (shown in Figure 4b) lined by the cap domain, which may facilitate the substrate entry and/or the product exit. To quantify the size of the active site in the WT and mutant enzymes, we calculated the binding pocket volumes using POVME 2.0 (32). The average pocket volume in the wild type simulation is 252 ± 43 Å^3, compared to 375 ± 67 Å^3 in W187H.

As shown in Figure 2b, the "20-loop" that connects α1 and α2 and the "200-loop" that connects α6 and α7 both show significant RMSF differences between the WT and W187H mutant enzymes. We further performed the principal component analysis (PCA) of the Cα atoms of the "20-loop" and the "200-loop" to investigate the underlying patterns in the atomic fluctuations of the cap domain with a reduced dimensionality. We computed eigenvectors (the components) from our data set, and each of those eigenvectors is associated

DOI: 10.1021/bi5015612
Biochemistry 2015, 54, 1841−1848

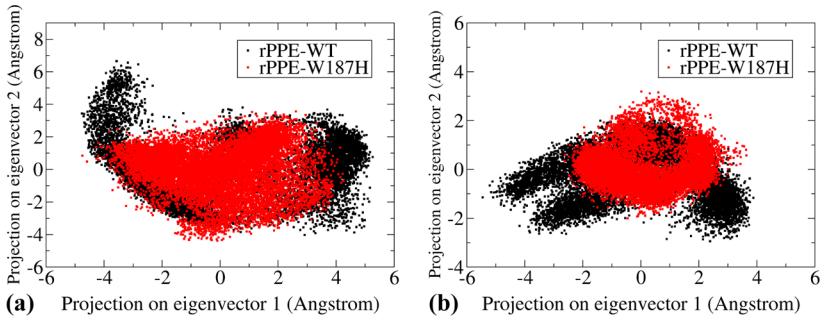

Figure 5. Projection of MD simulations of rPPE-WT and rPPE-W187H onto the corresponding first and second PC modes from the PCA analysis of the "20-loop" (a) and the "200-loop" (b) Cα atom fluctuations.

Table 1. Binding Energies of rPPE in Complex with (*S*)-AcO-CPA Computed Using the MM-PB/SA Method

energy (kcal/mol)	rPPE-WT	rPPE-W187H	rPPE-W187Y	rPPE-D287G
ΔE_{elec}	−4.8 ± 9.1	−47.1 ± 11.1	−9.5 ± 7.6	−116.4 ± 8.4
ΔE_{VDW}	−27.3 ± 2.1	−27.0 ± 2.9	−24.5 ± 2.1	−27.0 ± 2.7
$\Delta E_{PB,elec}$	32.5 ± 11.0	57.7 ± 10.8	23.8 ± 6.7	103.6 ± 5.6
$\Delta E_{nonpolar}$	−21.2 ± 0.9	−22.2 ± 1.0	−20.4 ± 0.7	−22.3 ± 0.5
ΔE_{disper}	35.6 ± 1.6	36.0 ± 1.2	34.8 ± 0.8	37.1 ± 0.8
ΔG_{bind}	14.8 ± 6.0	−2.7 ± 4.6	4.2 ± 3.5	−25.0 ± 5.3

with an eigenvalue, which tell us about how much variance there is in the data in that eigenvector direction. The first two components accounts for larger than 72.9% of the total variance. The MD trajectories of the two loops were then projected onto their respective first and second principal component modes as shown in Figure 5. The "20-loop" and "200-loop" in wild type are widely distributed, especially along the first PC mode, while W187H exhibits only modest variation along the two PC modes. Smaller fluctuations in both loops in W187H than WT are also observed in the corresponding apo systems (Figure S5). The two loops represent more stable outward conformation in W187H than WT. As both loops are located close to the entrance to the enzyme's active site, the differential flexibility of these loops should have a direct effect on the conformation of the substrate's accessible channel, and thus the enzyme's binding and activity.

Binding Free Energy Analysis. 1000 snapshots retrieved from the last 25 ns MD trajectories were used for the binding free energy calculations. The MM-PB(GB)/SA binding energy calculation results are listed in Tables 1 and S2. In these results, the entropic contributions to the binding free energy are ignored for two reasons. First, they are assumed to be similar among the different rPPE systems due to relatively small structural perturbations. Second and practically, quantitative entropy calculation remains a challenge for large biomolecular systems. Using the MM-PB/SA method, the calculated binding energy values are 14.8 ± 6.0 kcal/mol in the WT and −2.7 ± 4.6 kcal/mol in the W187H. With the MM-GB/SA method, the computed binding energies are −17.6 ± 2.5 kcal/mol in the WT and −28.0 ± 4.0 kcal/mol in the W187H. These calculated numbers may deviate from the corresponding experimental measurements due to various approximations used in the MM-PB(GB)/SA calculation, but the overall trend is consistent with the experimentally determined K_m values (146 mM in wild type versus 19.9 mM in the W187H mutant) listed in Table 2. The W187H mutant shows 1 order of magnitude increase in the substrate binding than the wild type enzyme. From the detailed decomposition of the total binding energy, the van der Waals interaction (ΔE_{VDW}) contributes more to the total binding energy than the electrostatic component ($\Delta E_{PB,elec}$), consistent with the observation that (*S*)-AcO-CPA makes more contacts with the W187H mutant than the WT enzyme. The decreased K_m thus improves the catalytic activity (k_{cat}/K_m) of the W187H mutant, whereas the rest improvement in the overall catalytic efficiency may arise from an increased k_{cat} due to the formation of a potentially more "active" near attack complex in W187H.

Table 2. Binding and Kinetic Parameters of Various rPPEs for Acetoxy Acid

enzyme	K_m (mM)	k_{cat} (s^{-1})	k_{cat}/K_m (mM^{-1} s^{-1})	references
rPPE-WT	146	8.9	0.0611	Ma et al.[10]
rPPE-W187H	19.9	123	6.20	Ma et al.[10]
rPPE-W187Y	301 ± 87	844 ± 169	2.81	this work
rPPE-D287G	18.3 ± 2.0	4.3 ± 0.1	0.23	this work

Rational Design and Experimental Verification. Our MD simulations showed that the imidazole moiety of His187 swings toward Asp256 and interacts with the side chains of Asp256 and Tyr288, leading to subsequent structural rearrangement of the active site that ultimately affects the substrate binding. On the basis of this observation, we speculate that residues that have a smaller aromatic ring than W187, such as phenylalanine and tyrosine, may undergo a similar conformational change, thus improve the enzyme's activity. Moreover, residues that have a smaller side chain than D287 may result in more space for the positional shift of His187 such that the substrate can bind more deeply and strongly in the binding pocket. Therefore, a smaller side chain in residue 287 may be important for overcoming steric clashes between the substrate and the enzyme, thus improve the substrate binding.

We further considered the conservation of individual residues in the rPPE family enzymes via the multiple sequence alignment method as shown in Figure S6.[36] Tyrosine is highly conserved in position 187 and glycine is highly conserved in position 287 in the esterases from different organisms. Moreover, the "SuSPect" estimation method using a support vector machine (SVM) algorithm[37] confirmed that both

DOI: 10.1021/bi5015612
Biochemistry 2015, 54, 1841−1848

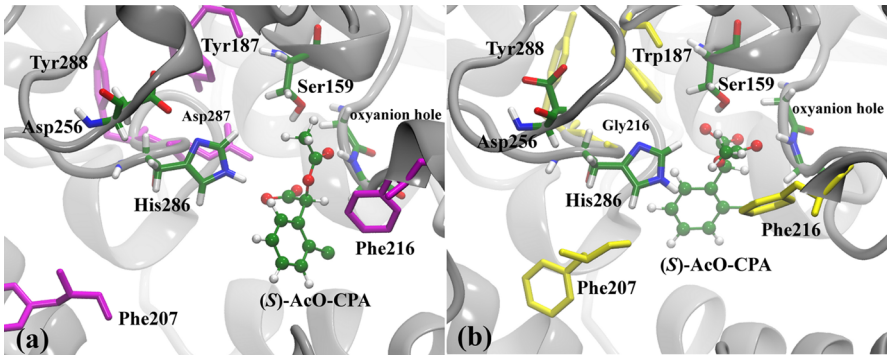

Figure 6. Binding modes of the substrate in the (a) W187Y and (b) D287G mutants. The catalytic triad and the substrate (*S*)-AcO-CPA are shown in green, and other relevant residues are shown in purple (W187Y) and in yellow (D287G), respectively.

positions 187 and 287 are highly conserved, with tyrosine more favorable than tryptophan in position 187, and glycine more favorable than aspartic acid in position 287. We subsequently generated the simulation systems for the two predicted mutants W187Y and D287G, and the MD simulations were carried out for about 50 ns to substantiate our prediction on their improved enzyme activity. rPPE-W187Y and rPPE-D287G were prepared using the same strategy as rPPE-WT. The apo W187Y and D287G structures were first generated from the APO-WT structure, which were then used to obtain ligand bound structures by Auto Dock Vina.

Similar to the other five systems, the simulations of rPPE-W187Y and rPPE-D287G have reached equilibrium after about 20 ns (Figure S7). From the surface view shown in Figure S8, it is clear that the cap domain assumes an "open" conformation in the W187Y mutant, similar to what has been observed in W187H. However, unlike in W187H, the "sandwich" structure no longer exists for the substrate binding in W187Y (Figure 6a), which may explain why the binding in W187Y has decreased when compared to that in W187H. The calculated binding energy for W187Y is 4.2 ± 3.5 kcal/mol using MM-PB/SA method and −18.9 ± 2.1 kcal/mol using MM-GB/SA method (Table 1, Table S2). These results suggest that W187Y increases the substrate binding as compared to the wild type, but decreases relative to the W187H mutant. In the D287G mutant, the substrate appears to bind more deeply to the binding pocket compared to the wild type (Figure 6b). The side chain of G287 is smaller and provides more room for the substrate to bind as predicted. The MM-PB(GB)/SA results for the D287G mutant are −25.0 ± 5.3 kcal/mol and −39.0 ± 3.5 kcal/mol respectively, indicating stronger substrate binding than the wild type and W187H mutants (Tables 1 and S2). Taken together, these calculations confirm that the two predicted residues (W187 and D287) may be considered as potential "hot spots" for mutagenesis screening to improve the catalytic efficiency of the enzyme.

Site-directed mutagenesis and biochemical assays were performed on the two predicted mutants W187Y and D287G to verify the binding and catalytic activity changes toward (*S*)-AcO-CPA (Table S3). We determined the binding and kinetic parameters of the purified mutant enzymes by measuring their activities under varying substrate concentrations (10−200 mM). As shown in Table 2, the overall catalytic activities of both W187Y and D287G are improved over that of the WT, but through different mechanisms. The Michaelis constant K_m is an inverse measure of the substrate's affinity for the enzyme with a small K_m indicating high affinity. The substrate binds a little less strongly to the W187Y mutant (K_m = 300) than to the WT (K_m = 146); therefore, the overall higher catalytic efficiency of W187Y than the WT is because the turnover number of W187Y (k_{cat} = 844) has increased by about 2 orders of magnitude than that of the WT (k_{cat} = 8.9). By contrast, D287G has an increased binding (K_m = 18.3) but a slightly decreased turnover number (k_{cat} = 4.3).

Discussion. With the availability of high-resolution structures of the enzyme−substrate complexes, structure-based molecular dynamics simulations can be carried out to unravel the molecular-level mechanisms of the substrate binding and catalysis, thus guiding rational design of the enzyme to improve its catalytic efficiency and stability. Our previous work reported that a recombinant carboxylesterase rPPE can hydrolyze racemic 2-acetoxy-2-(2′-chlorophenyl)-acetate with excellent (*S*)-enantioselectivity. Subsequently, the crystal structures of rPPE were determined.

In this work, we performed all-atom molecular dynamics simulations of the WT and several mutant rPPEs, both apo and in complex with the substrate (*S*)-AcO-CPA. The results show that the H187 mutation rearranges the active site so that the substrate binds more strongly and also is better positioned for the subsequent reaction in W187H than in the wild type, likely leading to the increased catalytic efficiency of the W187H mutant. In light of this observation together with additional binding free energy calculation results, we predicted that the mutants W187Y and D287G might improve the enzymatic efficiency through a similar mechanism. Further experiments verified that both W187Y and D287G mutants increase enzyme's catalytic efficiency, albeit through different mechanisms.

Although not entirely consistent with experimental validations, our computational work provides molecular insights into the binding of the substrate to carboxylesterase rPPEs; the binding free energy results obtained from MD simulations show a similar trend as those obtained experimentally, i.e., the substrate's binding affinity K_m. These results have helped identify potential sites for mutagenesis studies to rationally improve the enzyme's activity. However, it is worth noting that the substrate binding is only one side of a coin; the turnover rate k_{cat} is equally important in determining the overall catalytic activity of an enzyme. A full understanding of the detailed reaction mechanism (and determination of the associated reaction barriers and k_{cat}) of rPPEs will require a quantum mechanical/molecular mechanical (QM/MM) treatment of the system, which is beyond the scope of this paper and will be pursued in the future.

DOI: 10.1021/bi5015612
Biochemistry 2015, 54, 1841−1848

■ ASSOCIATED CONTENT

Supporting Information

Figure S1. The catalytic reaction of rPPE. Figure S2. RMSD and RMSF results of wild type and W187H mutant in apo form and the parallel system of wild type in complex with the substrate (*S*)-AcO-CPA. Figure S3. Binding mode of the substrate from the rPPE-WT-parallel simulation. Figure S4. The distance and angle of nucleophilic attack in wild type and in W187H mutant. Figure S5. Projection of MD simulations of APO-WT and APO-W187H onto the respective first and second PC modes from the PCA analysis of the "20-loop" and the "200-loop" Cα atom fluctuations. Figure S6. Multiple sequence alignment of the esterase from different organisms. Figure S7. RMSD and RMSF results of the W187Y and D287G rPPEs in complex with the substrate (*S*)-AcO-CPA. Figure S8. The surface view of the W187Y and D287G mutant rPPEs. This material is available free of charge via the Internet at http://pubs.acs.org.

■ AUTHOR INFORMATION

Corresponding Authors

*(X.C.) E-mail: chengx@ornl.gov.

*(J.-H.X.) E-mail: jianhexu@ecust.edu.cn.

Funding

This work is supported by the Postdoctoral Science Foundation of China (Grant No. 2014M551349), National Natural Science Foundation of China (No. 21276082), Ministry of Science and Technology, China (Nos. 2011CB710800 and 2011AA02A210), and China National Special Fund for State Key Laboratory of Bioreactor Engineering (No. 2060204). X.C. is partially supported by Computer Science and Mathematics Division at the Oak Ridge National Laboratory, which is managed by UT-Battelle, LLC under US DOE Contract No. De-AC05-00OR22725.

Notes

The authors declare no competing financial interest.

■ ACKNOWLEDGMENTS

We would like to thank State Key Laboratory of Microbial Metabolism at Shanghai Jiao Tong University and State Key Laboratory of Bioreactor Engineering at East China University for the computing resource support.

■ ABBREVIATIONS

rac-AcO-CPA, racemic 2-acetoxy-2-(2′-chlorophenyl)acetate; WT, wild type; MD, molecular dynamics; HSL, hormone sensitive lipase; CEs, carboxylesterases; MM-PB(GB)/SA, molecular Mechanics-Poisson Boltzmann (Generalized Born)/Surface Area; PCA, principal component analysis

■ REFERENCES

(1) Satoh, T., and Hosokawa, M. (2006) Structure, function and regulation of carboxylesterases. *Chem. Biol. Interact. 162*, 195−211.

(2) Bornscheuer, U. T. (2002) Microbial carboxyl esterases: classification, properties and application in biocatalysis. *FEMS Microbiol. Rev. 26*, 73−81.

(3) Martinez, D., Cutino-Avila, B., Perez, E. R., Menendez, C., Hernandez, L., and Del Monte-Martinez, A. (2014) A thermostable exo-beta-fructosidase immobilised through rational design. *Food Chem. 145*, 826−831.

(4) Zeng, Q. K., Du, H. L., Wang, J. F., Wei, D. Q., Wang, X. N., Li, Y. X., and Lin, Y. (2009) Reversal of coenzyme specificity and improvement of catalytic efficiency of Pichia stipitis xylose reductase by rational site-directed mutagenesis. *Biotechnol. Lett. 31*, 1025−1029.

(5) Irani, M., Tornvall, U., Genheden, S., Larsen, M. W., Hatti-Kaul, R., and Ryde, U. (2013) Amino acid oxidation of Candida antarctica lipase B studied by molecular dynamics simulations and site-directed mutagenesis. *Biochemistry 52*, 1280−1289.

(6) Yang, X. Q., Liu, J. Y., Li, X. C., Chen, M. H., and Zhang, Y. L. (2014) Key amino acid associated with acephate detoxification by Cydia pomonella carboxylesterase based on molecular dynamics with alanine scanning and site-directed mutagenesis. *J. Chem. Inf. Model. 54*, 1356−1370.

(7) Angkawidjaja, C., Koga, Y., Takano, K., and Kanaya, S. (2012) Structure and stability of a thermostable carboxylesterase from the thermoacidophilic archaeon Sulfolobus tokodaii. *FEBS J. 279*, 3071−3084.

(8) Ma, B. D., Yu, H. L., Pan, J., Liu, J. Y., Ju, X., and Xu, J. H. (2013) A thermostable and organic-solvent tolerant esterase from Pseudomonas putida ECU1011: catalytic properties and performance in kinetic resolution of alpha-hydroxy acids. *Bioresour. Technol. 133*, 354−360.

(9) Capodanno, D., Ferreiro, J. L., and Angiolillo, D. J. (2013) Antiplatelet therapy: new pharmacological agents and changing paradigms. *J. Thromb. Haemost. 11* (Suppl 1), 316−329.

(10) Ma, B.-D., Kong, X.-D., Yu, H.-L., Zhang, Z.-J., Dou, S., Xu, Y.-P., Ni, Y., and Xu, J.-H. (2014) Increased catalyst productivity in α-hydroxy acids resolution by esterase mutation and substrate modification. *ACS Catal. 4*, 1026−1031.

(11) Dou, S., Kong, X. D., Ma, B. D., Chen, Q., Zhang, J., Zhou, J., and Xu, J. H. (2014) Crystal structures of Pseudomonas putida esterase reveal the functional role of residues 187 and 287 in substrate binding and chiral recognition. *Biochem. Biophys. Res. Commun. 446*, 1145−1150.

(12) Holmquist, M. (2000) Alpha/Beta-hydrolase fold enzymes: structures, functions and mechanisms. *Curr. Protein Pept Sci. 1*, 209−235.

(13) Streit, T. M., Borazjani, A., Lentz, S. E., Wierdl, M., Potter, P. M., Gwaltney, S. R., and Ross, M. K. (2008) Evaluation of the 'side door' in carboxylesterase-mediated catalysis and inhibition. *Biol. Chem. 389*, 149−162.

(14) Wierdl, M., Morton, C. L., Nguyen, N. K., Redinbo, M. R., and Potter, P. M. (2004) Molecular modeling of CPT-11 metabolism by carboxylesterases (CEs): use of pnb CE as a model. *Biochemistry 43*, 1874−1882.

(15) Yu, X., Sigler, S. C., Hossain, D., Wierdl, M., Gwaltney, S. R., Potter, P. M., and Wadkins, R. M. (2012) Global and local molecular dynamics of a bacterial carboxylesterase provide insight into its catalytic mechanism. *J. Mol. Model. 18*, 2869−2883.

(16) Trott, O., and Olson, A. J. (2010) AutoDock Vina: improving the speed and accuracy of docking with a new scoring function, efficient optimization, and multithreading. *J. Comput. Chem. 31*, 455−461.

(17) Wang, J., Wang, W., Kollman, P. A., and Case, D. A. (2001) Antechamber: an accessory software package for molecular mechanical calculations. *J. Am. Chem. Soc. 222*, U403.

(18) Jorgensen, W. L., Chandrasekhar, J., Madura, J. D., Impey, R. W., and Klein, M. L. (1983) Comparison of simple potential functions for simulating liquid water. *J. Chem. Phys. 79*, 926−935.

(19) Hornak, V., Abel, R., Okur, A., Strockbine, B., Roitberg, A., and Simmerling, C. (2006) Comparison of multiple Amber force fields and development of improved protein backbone parameters. *Proteins 65*, 712−725.

(20) Case, D. A., Cheatham, T. E., 3rd, Darden, T., Gohlke, H., Luo, R., Merz, K. M., Jr., Onufriev, A., Simmerling, C., Wang, B., and Woods, R. J. (2005) The Amber biomolecular simulation programs. *J. Comput. Chem. 26*, 1668−1688.

(21) Frisch, M. J., Trucks, G. W., Schlegel, H. B., Scuseria, G. E., Robb, M. A., Cheeseman, J. R., Montgomery, Jr., J. A., Vreven, T., Kudin, K. N., Burant, J. C., Millam, J. M., Iyengar, S. S., Tomasi, J., Barone, V., Mennucci, B., Cossi, M., Scalmani, G., Rega, N., Petersson,

DOI: 10.1021/bi5015612
Biochemistry 2015, 54, 1841−1848

G. A., Nakatsuji, H., Hada, M., Ehara, M., Toyota, K., Fukuda, R., Hasegawa, J., Ishida, M., Nakajima, T., Honda, Y., Kitao, O., Nakai, H., Klene, M., Li, X., Knox, J. E., Hratchian, H. P., Cross, J. B., Bakken, V., Adamo, C., Jaramillo, J., Gomperts, R., Stratmann, R. E., Yazyev, O., Austin, A. J., Cammi, R., Pomelli, C., Ochterski, J. W., Ayala, P. Y., Morokuma, K., Voth, G. A., Salvador, P., Dannenberg, J. J., Zakrzewski, V. G., Dapprich, S., Daniels, A. D., Strain, M. C., Farkas, O., Malick, D. K., Rabuck, A. D., Raghavachari, K., Foresman, J. B., Ortiz, J. V., Cui, Q., Baboul, A. G., Clifford, S., Cioslowski, J., Stefanov, B. B., Liu, G., Liashenko, A., Piskorz, P., Komaromi, I., Martin, R. L., Fox, D. J., Keith, T., Al-Laham, M. A., Peng, C. Y., Nanayakkara, A., Challacombe, M., Gill, P. M. W., Johnson, B., Chen, W., Wong, M. W., Gonzalez, C., Pople, J. A. (2004) *Gaussian 03*, revision c. 02; Gaussian Inc., Wallingford, CT.

(22) Phillips, J. C., Braun, R., Wang, W., Gumbart, J., Tajkhorshid, E., Villa, E., Chipot, C., Skeel, R. D., Kale, L., and Schulten, K. (2005) Scalable molecular dynamics with NAMD. *J. Comput. Chem. 26*, 1781−1802.

(23) Darden, T., York, D., and Pedersen, L. (1993) Particle mesh Ewald: An N· log (N) method for Ewald sums in large systems. *J. Chem. Phys. 98*, 10089−10092.

(24) Pronk, S., Pall, S., Schulz, R., Larsson, P., Bjelkmar, P., Apostolov, R., Shirts, M. R., Smith, J. C., Kasson, P. M., van der Spoel, D., Hess, B., and Lindahl, E. (2013) GROMACS 4.5: a high-throughput and highly parallel open source molecular simulation toolkit. *Bioinformatics 29*, 845−854.

(25) Grant, B. J., Rodrigues, A. P., ElSawy, K. M., McCammon, J. A., and Caves, L. S. (2006) Bio3d: an R package for the comparative analysis of protein structures. *Bioinformatics 22*, 2695−2696.

(26) Humphrey, W., Dalke, A., and Schulten, K. (1996) VMD: visual molecular dynamics. *J. Mol. Graph 14* (33−38), 27−38.

(27) Kollman, P. A., Massova, I., Reyes, C., Kuhn, B., Huo, S., Chong, L., Lee, M., Lee, T., Duan, Y., Wang, W., Donini, O., Cieplak, P., Srinivasan, J., Case, D. A., and Cheatham, T. E., 3rd. (2000) Calculating structures and free energies of complex molecules: combining molecular mechanics and continuum models. *Acc. Chem. Res. 33*, 889−897.

(28) Chen, Q., Buolamwini, J. K., Smith, J. C., Li, A., Xu, Q., Cheng, X., and Wei, D. (2013) Impact of resistance mutations on inhibitor binding to HIV-1 integrase. *J. Chem. Inf. Model. 53*, 3297−3307.

(29) Gallicchio, E., and Levy, R. M. (2011) Recent theoretical and computational advances for modeling protein-ligand binding affinities. *Adv. Protein Chem. Struct. Biol. 85*, 27−80.

(30) Laskowski, R. A., and Swindells, M. B. (2011) LigPlot+: multiple ligand-protein interaction diagrams for drug discovery. *J. Chem. Inf. Model. 51*, 2778−2786.

(31) Cygler, M., Schrag, J. D., Sussman, J. L., Harel, M., Silman, I., Gentry, M. K., and Doctor, B. P. (1993) Relationship between sequence conservation and three-dimensional structure in a large family of esterases, lipases, and related proteins. *Protein Sci. 2*, 366−382.

(32) Frey, P. A., Whitt, S. A., and Tobin, J. B. (1994) A low-barrier hydrogen bond in the catalytic triad of serine proteases. *Science 264*, 1927−1930.

(33) Bruice, T. C., and Lightstone, F. C. (1999) Ground state and transition state contributions to the rates of intramolecular and enzymatic reactions. *Acc. Chem. Res. 32*, 127−136.

(34) Mandrich, L., Merone, L., Pezzullo, M., Cipolla, L., Nicotra, F., Rossi, M., and Manco, G. (2005) Role of the N terminus in enzyme activity, stability and specificity in thermophilic esterases belonging to the HSL family. *J. Mol. Biol. 345*, 501−512.

(35) Park, S. Y., Lee, S. H., Lee, J., Nishi, K., Kim, Y. S., Jung, C. H., and Kim, J. S. (2008) High-resolution structure of ybfF from Escherichia coli K12: a unique substrate-binding crevice generated by domain arrangement. *J. Mol. Biol. 376*, 1426−1437.

(36) Larkin, M. A., Blackshields, G., Brown, N. P., Chenna, R., McGettigan, P. A., McWilliam, H., Valentin, F., Wallace, I. M., Wilm, A., Lopez, R., Thompson, J. D., Gibson, T. J., Higgins, D. G. (2007) Clustal W and Clustal X version 2.0, *Bioinformatics 23*, 2947−2948.

(37) Yates, C. M., Filippis, I., Kelley, L. A., and Sternberg, M. J. (2014) SuSPect: enhanced prediction of single amino acid variant (SAV) phenotype using network features. *J. Mol. Biol. 426*, 2692−2701.

DOI: 10.1021/bi5015612
Biochemistry 2015, 54, 1841−1848